



## Research article

# Low temperature synthesis of MCM-48 and its adsorbent capacity for the removal of basic red 29 dye from model solutions

Yeşim Güçbilmez<sup>a,\*</sup>, Yusuf Yavuz<sup>b</sup>, İbrahim Çalış<sup>c</sup>, A. Şeyda Yargıç<sup>d</sup>,  
A. Savaş Koparal<sup>e</sup>

<sup>a</sup> Department of Chemical Engineering, ESTU, 26555, Eskisehir, Turkey

<sup>b</sup> Department of Environmental Engineering, ESTU, 26555, Eskisehir, Turkey

<sup>c</sup> Central Research Laboratory, Bartın University, 74100, Bartın, Turkey

<sup>d</sup> Department of Chemical Engineering, Bilecik Şeyh Edebalı University, 11230, Bilecik, Turkey

<sup>e</sup> Department of Health Programs, Anadolu University, 26555, Eskisehir, Turkey



## ARTICLE INFO

## Keywords:

Adsorption

Wastewater

MCM-48

Dye

Basic red 29

## ABSTRACT

The low temperature synthesis of MCM-48 was performed and its adsorptive properties were investigated for the first time in literature by studying Basic Red 29 (BR29) dye adsorption from model solutions. The modification of the surface properties and pore structure of silica-based material MCM-48 induced by BR29 adsorption were characterized using XRD, nitrogen physisorption, and SEM methods before and after dye adsorption.

The effects of contact time, solution pH, dye concentration, and temperature on the adsorption capacity of MCM-48 were investigated. Different adsorption models and different kinetic models were used, respectively to define the equilibrium data and the kinetics of adsorption. Adsorption data was seen to fit the Langmuir isotherm and the pseudo-second-order kinetic model. In addition, MCM-48 was found to be very successful for the removal of the BR29 dye model solutions, even at an initial dye concentration of 500 mg/L for which the removal efficiency was above 97%.

## 1. Introduction

Since the M41S family of mesoporous materials was discovered, substantial studies have been done on both their preparation and applications. The silica-based MCM-41, MCM-48, and MCM-50 are the three members of the M41S family, and they have hexagonal, cubic, and stabilized lamellar structures, respectively [1]. These so-called mesostructured materials have drawn a lot of interest from the scientific community over the last two decades. They were given certain qualities to give them in order to be used effectively in a range of applications, including chemical sensing, adsorption, and catalysis [2–10]. MCM-48 (Mobil Composite Material No. 48) type materials were found to be desirable adsorbents, catalysts and catalyst supports with high BET surface areas, narrow pore size distributions, and large pore volumes [11–15]. They have typically been utilized for the treatment of contaminants from wastewaters of different industries including the textile industry [16–22].

Significant quantities of wastewater from the textile industry might have strong colors, suspended particles, salts, a high pH, and a high chemical oxygen demand (COD) concentration. The first pollutant to be identified in wastewater is color. Water containing

\* Corresponding author.

E-mail address: [ygucebilmmez@eskisehir.edu.tr](mailto:ygucebilmmez@eskisehir.edu.tr) (Y. Güçbilmez).

relatively low levels of dyes (less than 1 ppm for certain dyes) is aesthetically offensive and very detectable. Additionally, many dye classes are stable compounds that can withstand exposure to light, chemicals, biological processes, and other factors without degrading, and thus are thought to be potential human carcinogens or mutagens [23,24]. A significant issue for the sector and a danger to the environment is the disposal of these colored wastewaters [25–27].

In the present study, The BR29 dye was removed from model solutions using a high surface area MCM-48 adsorbent, the influences of the initial pH, contact time, temperature, and initial dye concentration on the removal effectiveness were investigated. Surface characteristics and pore structure of MCM-48 were elucidated using XRD, nitrogen physisorption, and SEM methods before and after adsorption. The equilibrium isotherms were described using the Langmuir, Freundlich, Temkin, and Dubinin-Radushkevich adsorption models, while the kinetic data were defined utilizing pseudo-first/second-order and intraparticle diffusion models.

## 2. Materials and methods

TEOS (tetraethyl orthosilicate, 98% solution, Merck) was employed as the silica source, CTMABr (Cetyltrimethylammonium bromide, 99% purity, Merck) as the surfactant, ethanol (99.9% purity, Merck), and ammonium hydroxide (26% solution, Riedel de Haen) as the mineralizing agents and distilled water as the solvent medium for the synthesis of MCM-48. The adsorbent was produced at 30 °C by modifying the classical room temperature synthesis method [16] as follows: A clear surfactant solution was first prepared by solving CTMABr in 140 mL of distilled water at 30 °C by continuous stirring on a magnetic stirrer. Ethanol and ammonium hydroxide were added to this solution dropwise, respectively, and mixed for 10 min at the same temperature. Finally, 10 mL of TEOS was also mixed gently and a suspension with a molar composition of 1.0TEOS:0.4CTMABr:54EtOH:12.5NH<sub>4</sub>OH:174H<sub>2</sub>O at a pH value of 13.5 was obtained. The solid product obtained after stirring this suspension for two more hours at 30 °C was filtered and washed under vacuum until the filtrate's pH reached 7.0. The product was dried for 24 h at room temperature before being calcined in a tubular furnace. In the calcination process, the synthesized sample was heated from room temperature to 550 °C at a rate of 1 °C/min under a continuous flow of dry air moving at a rate of 1 L/min and was kept at 550 °C for 6 h. The adsorbent was kept in place during the calcination process despite the passage of dry air via a quartz membrane that was located in the center of the quartz tube. The as-synthesized material was then characterized by the XRD, BET, and SEM methods for the determination of the physical properties. Employing CuK $\alpha$  radiation ( $\lambda = 0.15406$  nm) on a Rigaku Rint 2000 diffractometer with a step size of 0.02 and scanning speed of 0.025 (2  $\theta$ /s) at 40 kV voltage and 30 mA current, XRD patterns of the MCM-48 adsorbent before and after adsorption tests were recorded. Nitrogen physisorption isotherms at 77 K were obtained in a Quantachrome Autosorb 1C instrument. Before the experiments, the purely siliceous samples were outgassed at 200 °C for 18 h, and the physisorption experiments were started at a point where the P/P<sub>0</sub> ratio was approximately 10<sup>-6</sup> to include any possible micropores present in the structure. The P/P<sub>0</sub> range of 0.05–0.30 was selected to calculate surface area values by using the BET (Brunauer-Emmett-Teller) equation, and the desorption branch of the isotherms was used to determine the pore size distributions and total pore volumes by applying the BJH (Barret-Joyner-Halenda) method. The Zeiss Supra 50 VP Microscope with 20 kV accelerating voltage and 7.5–10.5 mm working distance was applied to achieve the SEM and EDS results.

After the characterization procedures, adsorption experiments were performed to test the adsorptive capacity of the as-synthesized MCM-48. Model dye solutions with different initial concentrations were prepared using distilled water and the BR29 dye. The molecular formula and properties of the BR29 dye are listed in Table 1. For each adsorption experiment, 0.1 g of MCM-48 was added into 100 mL of the model solution. To analyze the BR29 concentrations, samples were taken from the reactor at predetermined time intervals, and they were then centrifuged at 7000 rpm. The as-synthesized purely siliceous adsorbent was called as MCM-48-LTS (MCM-48 Low Temperature Synthesis) and after dye adsorption it was called as MCM-48-BR29 (BR29 adsorbed MCM-48).

## 3. Results and discussion

This section contains the surface characteristics and pore structure of MCM-48, as determined by the XRD, nitrogen physisorption, SEM, and EDS studies before and after adsorption of the BR29 dye.

Results of the parametric investigations are also presented, including contact time, initial pH, temperature, and dye concentration. The Langmuir, Freundlich, Temkin, and Dubinin-Radushkevich isotherm models, which were used to study the adsorption equilibrium, are also included. Finally, the pseudo-first and second-order kinetics and intraparticle diffusion models utilized to explore the adsorption kinetics are illustrated.

Fig. 1 shows the XRD patterns of the MCM-48 adsorbent synthesized at 30 °C before and after BR29 adsorption. The original siliceous adsorbent, MCM-48-LTS, before the adsorption experiments, was seen to follow the typical XRD pattern of the MCM-48 type materials with the characteristic main peak around 2.72° and two secondary peaks indicating long-range order of cubic pores.

**Table 1**  
Properties of the BR29 dye.

Synonym	Basacryl Red GL
Molecular Formula	C <sub>19</sub> H <sub>17</sub> ClN <sub>4</sub> S
MW (g/mol)	368.88
$\lambda_{\max}$ (nm)	511
Source	Aldrich

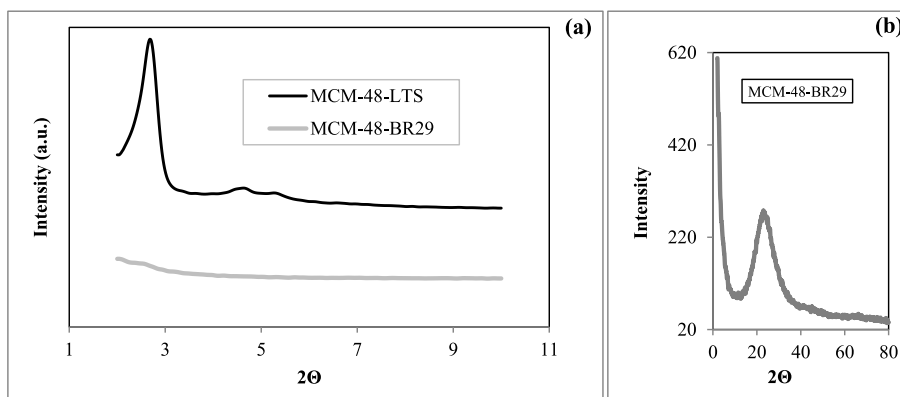


Fig. 1. XRD patterns of (a) MCM-48-LTS and MCM-48-BR29 in the  $2\theta$  range of  $2\text{--}10^\circ$  (b) MCM-48-BR29 in the  $2\theta$  range of  $2\text{--}80^\circ$ .

However, after dye adsorption, the MCM-48 structure was destroyed (Fig. 1a) and amorphous silica regions [28] were formed in the adsorbent represented by the large band centered around  $23.7^\circ$  in Fig. 1b.

Nitrogen physisorption analysis was also performed to determine how the adsorption of the BR29 dye affected the MCM-48 infrastructure. In Fig. 2, nitrogen physisorption isotherms are shown, while Fig. 3 presents the pore size distributions and Table 2 gives the BET surface areas, average BJH desorption pore diameters, and total pore volumes for MCM-48-LTS and MCM-48-BR29. The physisorption isotherms for MCM-48-LTS fit the IUPAC type IV model, which is common for ordered mesoporous silicate materials, as seen in Fig. 2 [29] and no significant hysteresis loop was formed indicating the presence of regular cylindrical pores [30–32]. After dye adsorption, however, MCM-48-

BR29 displayed the IUPAC type IV isotherms with a detectable H3 type hysteresis loop starting around  $P/P_0 = 0.40$  and ending around  $P/P_0 = 0.95$  indicating the formation of a complex network of various pore sizes as well pore blocking [20,23,24]. In addition, a dramatic increase in the amount of adsorbed nitrogen was seen after  $P/P_0 = 0.95$ , which is interpreted as the formation of macropores [33], the macropores are thought to be formed as a result of the pore networking effects [30,34].

As seen in Table 2 and Fig. 3a, the original adsorbent MCM-48-LTS had an average BJH desorption diameter of  $21.7 \text{ \AA}$  ( $2.17 \text{ nm}$ ), thus, its pore structure was mainly in the mesopore region, however after BR29 adsorption, as Fig. 3b depicts, various pore sizes could be detected. A close investigation of Fig. 3 shows that three peaks were obtained at  $24.3$ ,  $33.9$ , and  $48.4 \text{ \AA}$  ( $2.43$ ,  $3.39$ , and  $4.84 \text{ nm}$ ) with the largest peak corresponding to  $33.9 \text{ \AA}$  ( $3.39 \text{ nm}$ ). Thus, nitrogen physisorption results proved the shifting of pore sizes to higher diameters upon dye adsorption. This observation could be attributed to the insertion of part of the dye molecules in the silica walls, the consequent structure deterioration accompanied with pore enlargement, and resulting networking effects. Table 2 also depicts the reduction of BET surface area from  $1703 \text{ m}^2/\text{g}$  to  $543 \text{ m}^2/\text{g}$  and reduction of total pore volume from  $1.07 \text{ cm}^3/\text{g}$  to  $0.74 \text{ cm}^3/\text{g}$  upon BR29 adsorption. This reduction can be expressed by the blockage of pores by the dye molecules which were incorporated inside the mesopores or by the collapse of part of the amorphous silica walls into the meso-channels.

SEM images of MCM-48-LTS and MCM-48-BR29 are depicted in Fig. 4a and Fig. 4b, respectively. As seen, both adsorbents had spherical particles and homogeneous particle shape distributions. Thus, it is thought that most of the dye molecules were adsorbed inside the pores and silica walls of MCM-48-LTS rather than forming clusters on the outside surfaces of its particles. However, it was also seen that MCM-48-BR29 (Fig. 4b) had more spongy and larger particles.

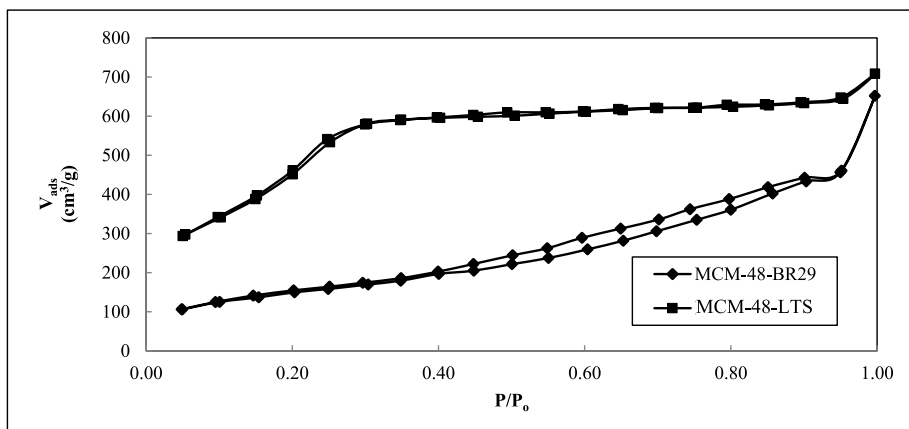


Fig. 2. Physisorption isotherms of the MCM-48 adsorbent prior to BR29 adsorption and after BR29 adsorption.

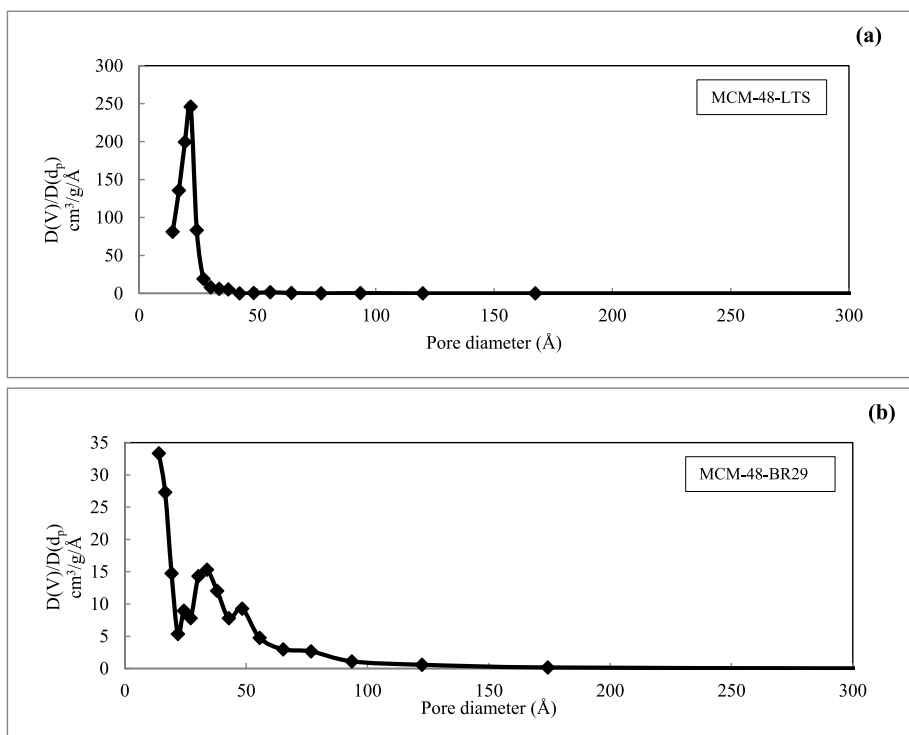


Fig. 3. Pore size distributions of MCM-48 (a) prior to BR29 adsorption (b) after BR29 adsorption.

Table 2

Surface area and pore size properties of MCM-48-LTS and MCM-48-BR29.

	MCM-48	MCM-48-BR29
BET Surface Area (m <sup>2</sup> /g)	1703	543
BJH Desorption Average Pore Diameter (nm)	2.17	Various diameters with the largest peak at 3.39 nm (Fig. 3)
Total Pore Volume (cm <sup>3</sup> /g)	1.08	0.74

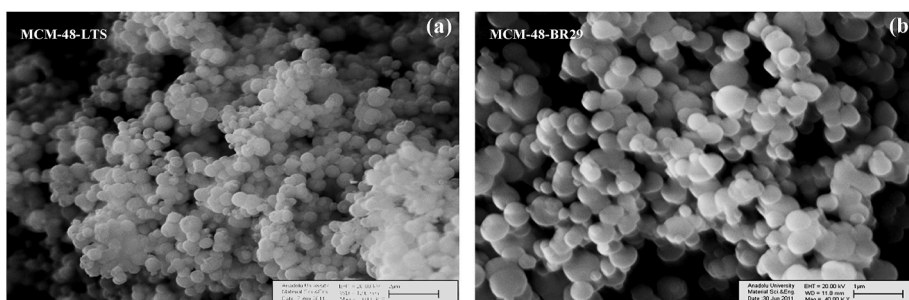


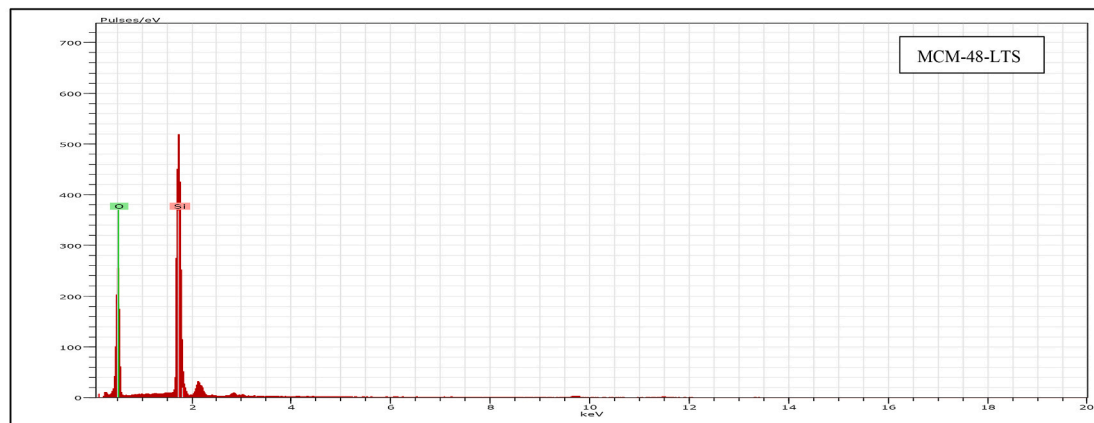
Fig. 4. SEM photographs of MCM-48 (a) prior to BR29 adsorption (b) after BR29 adsorption.

compared to MCM-48-LTS. The spongy appearance is thought to be due to the formation of new pores with the diameters of 3.39 and 4.84 nm as depicted in Fig. 3b and the pore networking effects [35,36]. In addition, the increase in particle size from approximately 0.3  $\mu\text{m}$  to 0.4  $\mu\text{m}$  after the adsorption experiments is thought to be due to some electrostatic interactions induced during the adsorption experiments [36].

A final analysis performed to prove dye adsorption into MCM-48-LTS was EDS analysis given in Fig. 5. This figure illustrates that before the adsorption experiments (Fig. 5a), MCM-48-LTS only contained Si and O atoms whereas the presence of C, Cl, N, and S atoms were detected in MCM-48-BR29 after dye adsorption (Fig. 5b).

**Spectrum: Acquisition** (a)

Element	unn. C [wt. %]	norm. C [wt. %]	Atom. C [at. %]	Compound Comp. C [wt. %]	norm. Comp. C [wt. %]	Error [%]
Silicon	27.59	31.25	20.57	31.25	27.59	1.2
Oxygen	60.70	68.75	79.43	68.75	60.70	7.9
<b>Total:</b>	<b>88.30</b>	<b>100.00</b>	<b>100.00</b>			



**Spectrum: Acquisition** (b)

Element	unn. C [wt. %]	norm. C [wt. %]	Atom. C [at. %]	Compound Comp. C [wt. %]	norm. Comp. C [wt. %]	Error [%]
Silicon	19.67	18.84	11.44	18.84	19.67	0.9
Oxygen	63.67	60.96	65.00	60.96	63.67	8.2
Carbon	4.87	4.66	6.62	4.66	4.87	1.2
Chlorine	0.77	0.73	0.35	0.73	0.77	0.1
Nitrogen	13.25	12.69	15.46	12.69	13.25	2.7
Sulfur	2.21	2.12	1.13	2.12	2.21	0.1
<b>Total:</b>	<b>104.44</b>	<b>100.00</b>	<b>100.00</b>			

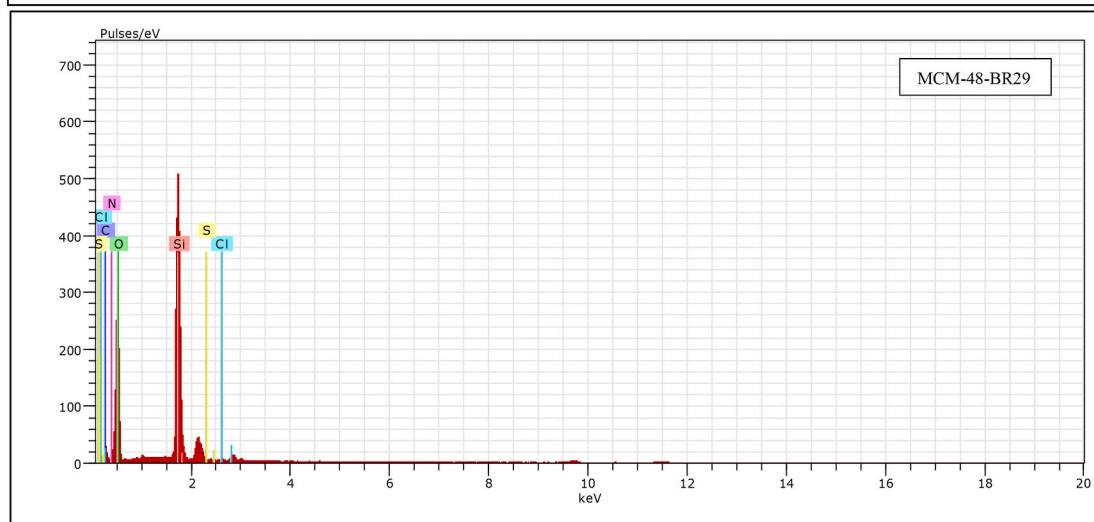


Fig. 5. EDS analysis results of MCM-48 (a) prior to BR29 adsorption (b) after BR29 adsorption.

### 3.1. Adsorption experiments

Seven initial pH values including the original pH (natural pH = 4.60) of the model solution were tested and the results obtained are shown in Fig. 6. Model solutions were set at various pH levels, spanning from 2.03 to 7.99, to ascertain the impact of pH on the adsorption capacity of MCM-48-LTS. According to Fig. 6, the adsorption capacity of BR29 onto MCM-48-LTS decreased only at the pH value of 2.03. Adsorption performance was almost similar at all other initial pH values studied. It was concluded that MCM-48-LTS was quite stable in a wide pH range. Hence, the natural pH was chosen as the best pH value since it was the most economical option which did not require addition of any extra acidic or basic chemicals.

MCM-48-LTS was found to be very efficient for the treatment of different initial BR29 concentrations varying from 50 to 500 mg/L as seen in Fig. 7. This figure illustrates that apparent adsorption equilibrium was obtained within 2 min for the initial BR29 concentrations of 50 mg/L and 100 mg/L. Besides, adsorption equilibria were reached within 10 min and 40 min for the initial BR29 concentrations of 200 mg/L and 500 mg/L, respectively. After the adsorption equilibrium, there were no discernible concentration fluctuations, and the average BR29 dye removal effectiveness for all initial concentrations examined was >97%. It was also clear that the time to reach the aforementioned decolorization yield was getting longer with the increasing dye concentration. It was believed that adsorption mostly occurred at surface locations that were simple to access, involving no diffusion into the micropores. The quick adsorption rate may also be caused by a hydrophobic contact between the adsorbent and the organic compound [37].

Since temperature is also an important parameter, decolorization efficiency versus time was recorded for different working temperatures as given in Fig. 8. Three different working temperatures (25, 45, and 65 °C) were studied. According to the results, the adsorption performance of the system was almost the same for the working temperatures of 25 °C (i.e., room temperature) and 45 °C. However, the removal efficiency increased until a given time period (30 min) at the working temperature of 65 °C and then exhibited a decreasing trend. This behavior of the system could be explained by the desorption process that might have been occurring around this temperature. The findings of the temperature research still made the adsorption process economical since the temperature adjustment was not necessary.

### 3.2. Adsorption isotherms and dynamics of BR29 adsorption onto MCM-48

To understand how the dye is adsorbed onto the adsorbent, to determine the maximum adsorption capacity, and to generate the most relevant correlations from the experimental results at equilibrium, adsorption isotherms are used. Although there are many different adsorption isotherm models available, the Freundlich and Langmuir models are the two that are most frequently recognized and utilized in the treatment of waters and effluents [13,38–40]. The Freundlich equation is an empirical equation used to represent heterogeneous systems and is not limited to the development of monolayers, in contrast to the Langmuir equation, which applies to homogeneous adsorption systems [41–43].

The Langmuir equation (Eq. 1) is expressed as:

$$\frac{C_e}{Q_e} = \frac{1}{Q_{\max}K_L} + \frac{C_e}{Q_{\max}} \quad (1)$$

In the Langmuir equation, the equilibrium BR29 concentration adsorbed on the adsorbent is denoted as  $Q_e$  (mg/g), the equilibrium BR29 concentration in the solution as  $C_e$  (mg/L), the monolayer adsorption capacity of MCM-48-LTS as  $Q_{\max}$  (mg/g), and  $K_L$  (L/mg) is the Langmuir adsorption constant. The concentration at which half the maximal adsorption capacity of the adsorbent is reached is given by the reciprocal value of the Langmuir constant  $K_L$ , which evaluates the affinity between the adsorbate and adsorbent. When the Langmuir model is accurate, a plot of  $C_e/Q_e$  vs  $C_e$  will result in a straight line with a slope of  $1/Q_{\max}$  and an intercept of  $1/Q_{\max}K_L$  [41]. Otherwise, the Freundlich equation (Eq. 2) is shown as:

$$Q_e = K_F C_e^{1/n} \quad (2)$$

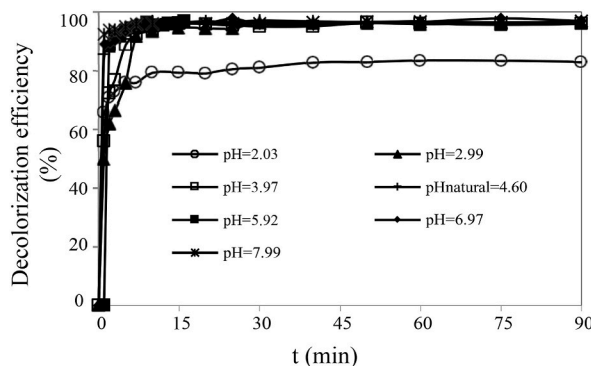


Fig. 6. Alteration of the decolorization efficiency with initial pH ( $C_0 = 200$  mg/L BR29).

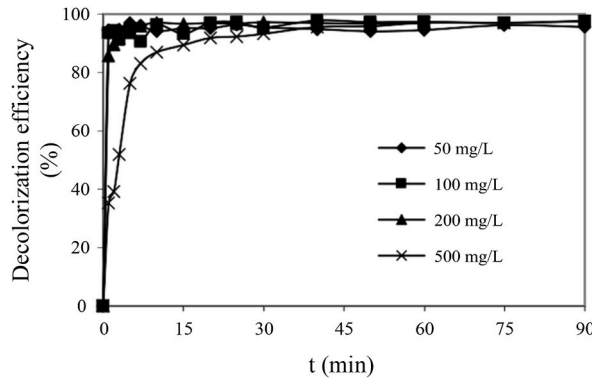


Fig. 7. Alteration of the decolorization efficiency with initial dye concentration (natural pH).

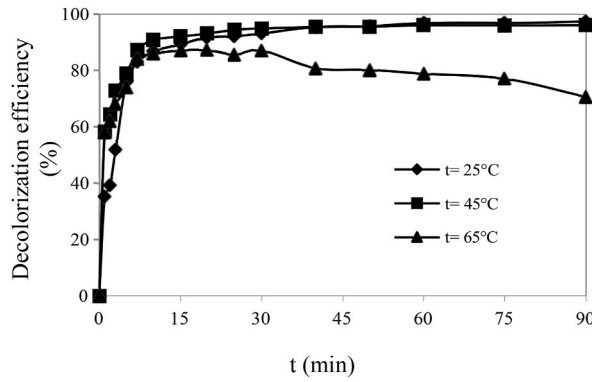


Fig. 8. Alteration of the decolorization efficiency with temperature ( $C_o = 500$  mg/L BR29, natural pH).

In the Freundlich equation, two Freundlich constants that relate to the adsorption capacity and adsorption intensity are denoted as  $K_F$  [ $\text{mg/g}(\text{L/g})^{1/n}$ ] and  $1/n$ , respectively. It is well acknowledged that a favourable adsorption and a rise in the adsorption capacity are associated with  $1/n < 1$  [44]. The plot of  $\ln Q_e$  vs  $\ln C_e$  is used to obtain the intercept  $K_F$  and slope  $1/n$ .

In addition to the basic models of Langmuir and Freundlich, Temkin and Dubinin-Radushkevich isotherm models can also be utilized to examine the equilibrium data. The equations used for the Dubinin-Radushkevich (Eqs. (3) and (4)) and Temkin (Eqs. (5) and (6)) models are as follows:

$$\ln Q_e = \ln Q_m - \beta \epsilon^2 \tag{3}$$

$$\epsilon = RT \ln(1 + 1 / C_e) \tag{4}$$

$$Q_e = B \ln AT + B \ln C_e \tag{5}$$

$$B = RT/b_t \tag{6}$$

In the Dubinin-Radushkevich equations,  $\epsilon$  and  $\beta$  denote the Polanyi potential and the constant concerned with the adsorption energy ( $\text{mol}^2/\text{kJ}^2$ ), respectively. The average adsorption energy (E) is computed from the expression  $1/\sqrt{2\beta}$  as kJ/mol. Following symbols are used in the Temkin model: Isotherm equilibrium binding constant ( $A_T$ , L/g), constant related to the heat of sorption (B), Temkin isotherm constant ( $b_t$ , J/mol), universal gas constant (R, J/molK), and absolute temperature (T, K) [45].

For the abovementioned isotherm models, experimental data collected at room temperature and natural pH for a BR29 concentration of 200 mg/L were used; natural pH was preferred since it was the most economical pH value for the given system. The isotherms are displayed in Fig. 9(a–d) and the values for the isotherm parameters of  $K_L$ ,  $Q_{\text{max}}$ ,  $K_F$ ,  $1/n$ ,  $A_T$ , B,  $b_t$ ,  $\beta$ , and E are given in Table 3. This table also includes the linear regression correlations for the Langmuir ( $r_L^2$ ), Freundlich ( $r_F^2$ ), Dubinin-Radushkevich ( $r_{DR}^2$ ), and Temkin ( $r_T^2$ ) isotherms. As can be seen, the Langmuir model better described the BR29 adsorption mechanism onto MCM-48-LTS since its linear regression correlation value ( $r_L^2$ ) was higher than those for the other isotherm models ( $r_F^2$ ,  $r_T^2$ , and  $r_{DR}^2$ ). Additionally,  $Q_{\text{max}}$  for the initial BR29 concentration of 200 mg/L was calculated as 500 mg/g with a correlation coefficient ( $r_L^2$ ) of 0.9986. The value of  $1/n$  was confirmed to be less than 1.0 when the Freundlich model was taken into account, suggesting strong adsorption intensity.

As seen in Table 3, the average energy of adsorption estimated using the Dubinin-Radushkevich isotherm model was 0.2957 kJ/

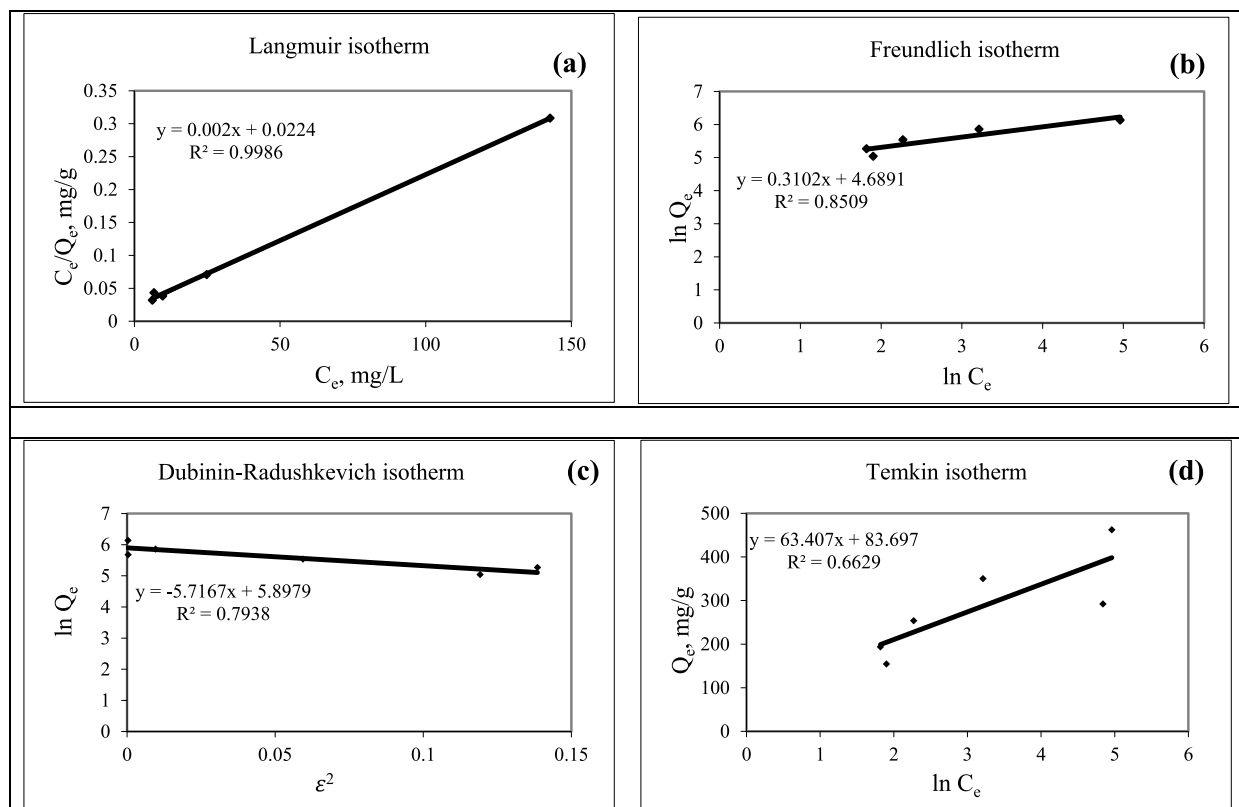


**Fig. 9.** Fitting (a) Langmuir, (b) Freundlich, (c) Dubinin-Radushkevich, and (d) Temkin models to the adsorption isotherms of MCM-48-BR29 ( $C_0 = 200$  mg/L BR29, natural pH, room temperature).

**Table 3**

Isotherm constants for the adsorption of BR29 onto MCM-48 ( $C_0 = 200$  mg/L BR29, natural pH, room temperature).

Model	Parameters	Adsorption via MCM-48
Langmuir model	$r_L^2$	0.9986
	$Q_{max}$ (mg/g)	500
Freundlich model	$K_L$ (L/mg)	0.089
	$r_F^2$	0.8509
	$1/n$	0.31
Temkin model	$K_T$ [mg/g(L/g) $^{1/n}$ ]	108.75
	$r_T^2$	0.6629
	$B$	63.407
	$b_T$ (J/mol)	0.0256
Dubinin- Radushkevich model	$A_T$ (L/g)	3.7434
	$r_{DR}^2$	0.7938
	$q_m$ (mg/g)	364.27
	$\beta$ (mol $^2$ /kJ $^2$ )	5.7200
	$E$ (kJ/mol)	0.2957

mol. It is known that, for this model, the physical and chemical mechanism of adsorption can be analyzed by calculating the average energy of the process ( $E$ , kJ/mol): Physical forces are effective on adsorption when  $E < 8$  kJ/mol, particle diffusion is effective when  $E > 16$  kJ/mol, and adsorption originates via the ion exchange mechanism for  $8 < E < 16$  kJ/mol [46]. Accordingly, it was found that for the BR29 adsorption on MCM-48-LTS, physical forces were effective.

Kinetic studies were also performed to define the rate law of BR29 uptake from model solutions using the MCM-48-LTS adsorbent. The pseudo-first and second order, and intraparticle diffusion kinetic models were tested for which the corresponding rate laws are given in Eqs. (7)–(9) [47–49]:

$$\log(Q_e - Q_t) = \log Q_e - (k_1 t) / 2.303 \tag{7}$$

$$t / Q_t = 1 / (k_2 Q_e^2) + (1 / Q_e) t \tag{8}$$

$$Q_t = k_i t^{1/2} + C \quad (9)$$

The amounts of BR29 adsorbed at equilibrium and at time  $t$  (min) are denoted by  $Q_e$  (mg/g) and  $Q_t$  (mg/g), the equilibrium rate constants of the pseudo-first and second order adsorption are  $k_1$  ( $\text{min}^{-1}$ ) and  $k_2$  (g/mg-min), the rate constant of intraparticle diffusion is  $k_i$ , and  $C$  is the intercept. The  $\log(Q_e - Q_t)$  vs  $t$  and  $t/Q_t$  vs  $t$  plots are used to determine the values of the rate constants and  $Q_e$  for the pseudo-first and second-order kinetic models, respectively. In the case of the intraparticle diffusion kinetic model,  $k_i$  is calculated from the slope of the  $Q_t$  (mg/g) versus  $t^{1/2}$  ( $\text{min}^{1/2}$ ) plot.

The experimental adsorption data plotted using Eqs (7)–(9) are given in Fig. 10(a–c) while the values of the fitted model parameters and the correlation coefficients are given in Table 4. This table depicts that when the experimental data was plotted using Equation (8), the pseudo-second order model yielded a linear regression coefficient greater than 0.99. Thus, it is concluded that the adsorption of BR29 onto MCM-48-LTS follows pseudo-second order kinetics.

#### 4. Conclusions

In this study, a high surface area MCM-48 adsorbent was prepared by a low temperature synthesis method at 30 °C. The as-synthesized adsorbent was found to be very effective in BR29 dye adsorption from model solutions. XRD,  $\text{N}_2$  physisorption, and SEM techniques were performed in order to determine the modification of the surface characteristics and pore structure upon dye adsorption. Nitrogen physisorption results depicted a significant reduce in the specific surface area and pore volume while the XRD patterns illustrated that dye adsorption destroyed the cubic mesoporous infrastructure and a more complex structure with various pore sizes was formed. The adsorption capacity of MCM-48 was explored by performing experiments at different initial pH values, initial dye concentrations, and temperatures. The best pH value was found as the natural pH and the adsorbent was found to be very efficient for the treatment of different initial BR29 concentrations varying from 50 to 500 mg/L with an average removal efficiency of >97%. Adsorption performance was found to be almost identical for the temperatures of 25 and 45 °C while removal efficiency decreased after 30 min at 65 °C. The equilibrium data were fitted using the Langmuir, Freundlich, Temkin, and Dubinin-Radushkevich isotherm models, and it was revealed that the Langmuir model best qualified the adsorption process. Finally, the adsorption kinetics was seen to

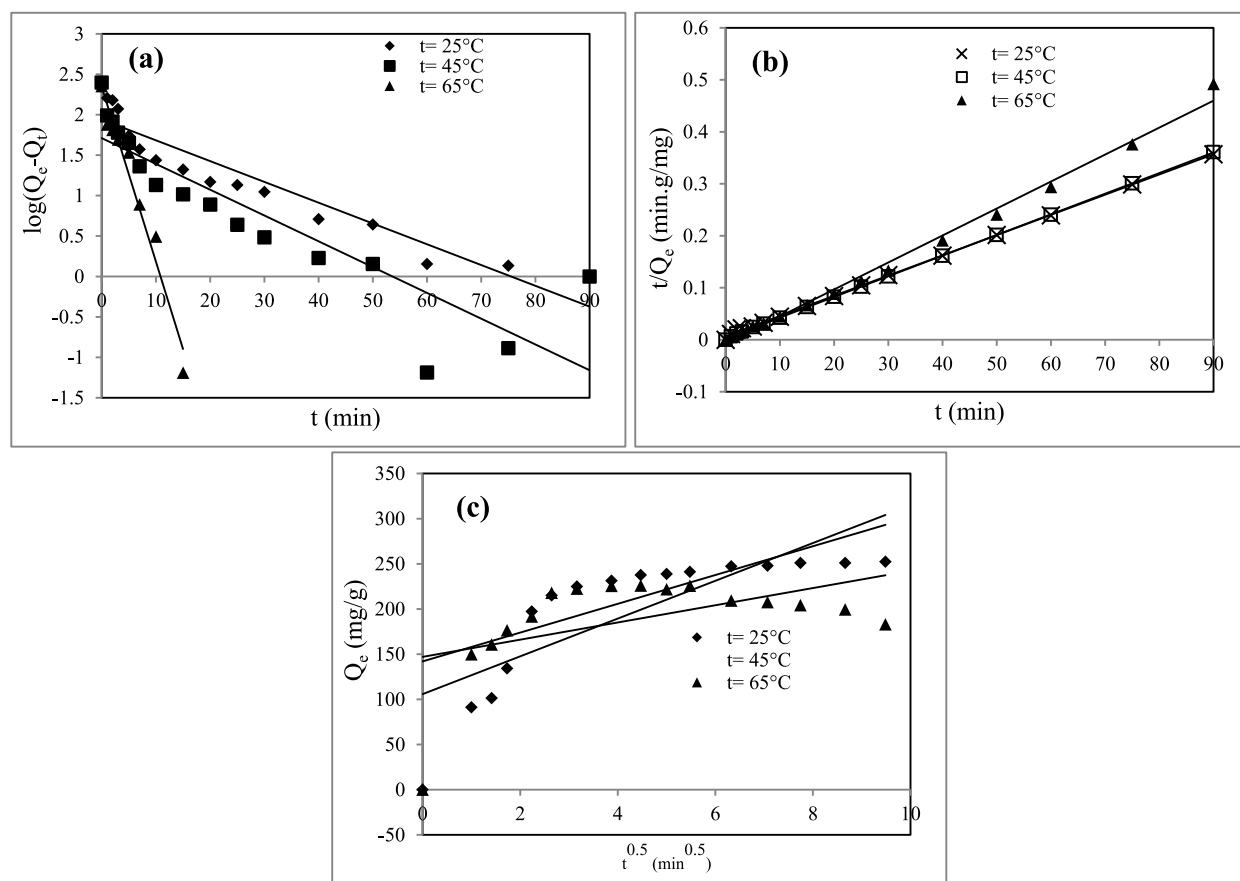


**Fig. 10.** Kinetic models for the adsorption of BR29 onto MCM-48-LTS: (a) pseudo-first order model, (b) pseudo-second order model, and (c) intraparticle diffusion model ( $C_0 = 500$  mg/L BR29, natural pH).

**Table 4**Kinetic model parameters for the adsorption of BR29 onto MCM-48 ( $C_0 = 500$  mg/L BR29, natural pH).

	T (°C)	25	45	65
Pseudo-first-order	$r^2$	0.8938	0.7833	0.9628
	$q_{e,calc}$ (mg/g)	87.19	51.38	221.16
	$k_1$ ( $\text{min}^{-1}$ )	0.0592	0.0735	0.4977
Pseudo-second-order	$\frac{2}{r}$	0.9995	0.9999	0.9934
	$Q_e$ (mg/g)	256.41	250.00	192.31
	$k_2$ (g/mg.min)	0.0023	0.0055	0.0038
Intraparticle diffusion	$r^2$	0.6404	0.5033	0.2423
	C	105.75	141.98	146.98
	$k_i$ (mg/g $\cdot$ min <sup>0.5</sup> )	20.9060	15.9340	9.5201

follow pseudo-second order kinetics.

### Funding statement

This work was supported by the Scientific Research Projects BAP 1003F97 and BAP 1106F120 of Anadolu University.

### References

- [1] J.S. Beck, J.C. Vartuli, W.J. Roth, M.E. Leonowicz, C.T. Kresge, K.D. Schmitt, C.T.-W. Chu, K.H. Olson, E.W. Sheppard, S.B. McCullen, J.B. Higgins, J.L. J. Schlenker, A new family of mesoporous molecular sieves prepared with liquid crystal templates, *J. Am. Chem. Soc.* 114 (1992) 10834–10843, <https://doi.org/10.1021/ja00053a020>.
- [2] R. Saad, K. Belkacemi, S. Hamoudi, Adsorption of phosphate and nitrate anions on ammonium-functionalized MCM-48: effects of experimental conditions, *J. Colloid Interface Sci.* 311 (2007) 375–381, <https://doi.org/10.1016/j.jcis.2007.03.025>.
- [3] Z. Allothman, A review: fundamental aspects of silicate mesoporous materials, *Mater* 5 (2012) 2874–2902, <https://doi.org/10.3390/ma5122874>.
- [4] J.A.S. Costa, R.A. de Jesus, D.O. Santos, J.F. Mano, L.P.C. Romão, C.M. Paranhos, Recent progresses in the adsorption of organic, inorganic, and gas compounds by MCM-41-based mesoporous materials, *Microporous Mesoporous Mater.* 291 (2020), 109698, <https://doi.org/10.1016/j.micromeso.2019.109698>.
- [5] J.A.S. Costa, R.A. de Jesus, D.O. Santos, J.B. Neris, R.T. Figueiredo, C.M. Paranhos, Synthesis, functionalization, and environmental application of silica-based mesoporous materials of the M41S and SBA-n families: a review, *J. Environ. Chem. Eng.* 9 (3) (2021), 105259, <https://doi.org/10.1016/j.jece.2021.105259>.
- [6] S.W. Machado, J.C. Santana, A.M. Pedrosa, M.J. Souza, A.C. Coriolano, E.K. Morais, A.S. Araujo, Catalytic cracking of isopropylbenzene over hybrid HZSM-12/M41S (M41S= MCM-41 or MCM-48) micro-mesoporous materials, *Petrol. Sci. Technol.* 36 (13) (2018) 923–929, <https://doi.org/10.1080/10916466.2018.1454950>.
- [7] F. Gao, H. Zhou, Z. Shen, H. Qiu, L. Hao, H. Chen, X. Zhou, Synergistic antimicrobial activities of tea tree oil loaded on mesoporous silica encapsulated by polyethyleneimine, *J. Dispersion Sci. Technol.* 41 (12) (2020) 1859–1871, <https://doi.org/10.1080/01932691.2019.1637755>.
- [8] C. Cara, E. Rombi, V. Mameli, A. Ardu, M. Sanna Angotzi, D. Niznansky, A. Musinu, C. Cannas,  $\gamma$ -Fe<sub>2</sub>O<sub>3</sub>-M41S sorbents for H<sub>2</sub>S removal: effect of different porous structures and silica wall thickness, *J. Phys. Chem. C* 122 (23) (2018) 12231–12242, <https://doi.org/10.1021/acs.jpcc.8b01487>.
- [9] N. Morin-Crini, M. Fourmentin, S. Fourmentin, G. Torri, G. Crini, Synthesis of silica materials containing cyclodextrin and their applications in wastewater treatment, *Environ. Chem. Lett.* 17 (2) (2019) 683–696, <https://doi.org/10.1007/s10311-018-00818-0>.
- [10] J.A.S. Costa, V.C. Costa, M.L. de Mello, C.M. Paranhos, Application of the experimental design in the optimization of a procedure for antimony (Sb) remediation in environmental samples employing mesoporous array, *Environ. Sci. Pollut. Res.* 29 (8) (2022) 11172–11184, <https://doi.org/10.1007/s11356-021-16414-9>.
- [11] K. Schumacher, M. Grün, K.K. Unger, Novel synthesis of spherical MCM-48, *Microporous Mesoporous Mater.* 27 (1999) 201–206, [https://doi.org/10.1016/S1387-1811\(98\)00254-6](https://doi.org/10.1016/S1387-1811(98)00254-6).
- [12] W. Zhao, Z. Hao, C. Hu, Synthesis of MCM-48 with a high thermal and hydro-thermal stability, *Mater. Res. Bull.* 40 (2005) 1775–1780, <https://doi.org/10.1016/j.materresbull.2005.05.012>.
- [13] A.K. Basumaty, P.V. Singh, R.V. Kumar, A.K. Ghoshal, G. Pugazhenthii, Development and characterization of a MCM-48 ceramic composite membrane for the removal of Cr(VI) from an aqueous solution, *J. Environ. Eng.* 142 (9) (2016), [https://doi.org/10.1061/\(ASCE\)EE.1943-7870.0000993](https://doi.org/10.1061/(ASCE)EE.1943-7870.0000993).
- [14] A.R.D. Nascimento, R.L.B.D.A. Medeiros, M.A.D.F. Melo, D.M.D.A. Melo, M.J.B.D. Souza, Optimization of MCM-48 synthesis using factorial design, *Cerâmica* 62 (2016) 413–417, <https://doi.org/10.1590/0366-69132016623642028>.
- [15] S. Ahmad, K. Yasin, A.T. Shah, Catalytic oxidation of toluene using Co-MCM-48 and CoMn-MCM-48 mesoporous material, *J. Chem. Soc. Pak.* 40 (2018) 95–100.
- [16] C. Zubieta, M.B. Sierra, M.A. Morini, P.C. Schulz, L. Albertengo, M.S. Rodríguez, The adsorption of dyes used in the textile industry on mesoporous materials, *Colloid Polym. Sci.* 286 (2008) 377–384, <https://doi.org/10.1007/s00396-007-1777-7>.
- [17] M. Shaban, M.R. Abukhadra, A. Hamd, R.R. Amin, A.A. Khalek, Photocatalytic removal of Congo red dye using MCM-48/Ni<sub>2</sub>O<sub>3</sub> composite synthesized based on silica gel extracted from rice husk ash; fabrication and application, *J. Environ. Manag.* 204 (2017) 189–199, <https://doi.org/10.1016/j.jenvman.2017.08.048>.
- [18] P. Taba, N. Shintadewi, M. Zakir, P. Budi, Removal of brilliant scarlet by MCM-48 materials, *IOP Conf. Ser. Earth Environ. Sci.* 473 (2020), 012126, <https://doi.org/10.1088/1755-1315/473/1/012126>.
- [19] M. Shaban, A. Hamd, R.R. Amin, M.R. Abukhadra, A.A. Khalek, A.A.P. Khan, A.M. Asiri, Preparation and characterization of MCM-48/nickel oxide composite as an efficient and reusable catalyst for the assessment of photocatalytic activity, *Environ. Sci. Pollut. Res.* 27 (26) (2020) 32670–32682, <https://doi.org/10.1007/s11356-020-09431-7>.
- [20] M.R. Abukhadra, M. Shaban, Recycling of different solid wastes in synthesis of high-order mesoporous silica as adsorbent for safranin dye, *Int. J. Environ. Sci. Technol.* 16 (11) (2019) 7573–7582, <https://doi.org/10.1007/s13762-019-02231-8>.
- [21] H.I. Meléndez-Ortiz, B. Puente-Urbina, J.A. Mercado-Silva, L. García-Urioste, Adsorption performance of mesoporous silicas towards a cationic dye. Influence of mesostructure on adsorption capacity, *Int. J. Appl. Ceram. Technol.* 16 (4) (2019) 1533–1543, <https://doi.org/10.1111/ijac.13179>.
- [22] S.M. Alardhi, J.M. Alrubaye, T.M. Albayati, Adsorption of Methyl Green dye onto MCM-41: equilibrium, kinetics and thermodynamic studies, *Desalination Water Treat.* 179 (2020) 323–331, <https://doi.org/10.5004/dwt.2020.25000>.
- [23] Q. Qin, J. Ma, K. Liu, Adsorption of anionic dyes on ammonium-functionalized MCM-41, *J. Hazard Mater.* 162 (2009) 133–139, <https://doi.org/10.1016/j.jhazmat.2008.05.016>.
- [24] G.A.R. de Oliveira, D.M. Leme, J. de Lapuente, L.B. Brito, C. Porredón, L. de B. Rodrigues, N. Brull, J.T. Serret, M. Borràs, G.R. Disner, M.M. Cestari, D.P. de Oliveira, A test battery for assessing the ecotoxic effects of textile dyes, *Chem. Biol. Interact.* 291 (2018) 171–179, <https://doi.org/10.1016/j.cbi.2018.06.026>.
- [25] Y. Yavuz, A.S. Kopalal, Ü.B. Ögütveren, Electrochemical oxidation of Basic Blue 3 dye by using diamond anode: evaluation of color, COD and toxicity removal, *J. Chem. Technol. Biotechnol.* 86 (2011) 261–265, <https://doi.org/10.1002/jctb.2512>.
- [26] M.A. Hassaan, A. El Nemr, Health and environmental impacts of dyes: mini review, *Am. J. Environ. Sci.* 1 (2017) 64–67, <https://doi.org/10.11648/j.ajese.20170103.11>.

- [27] B. Lellis, C.Z. Fávoro-Polonio, J.A. Pamphile, J.C. Polonio, Effects of textile dyes on health and the environment and bioremediation potential of living organisms, *Biotechnol. Res. Innov.* 3 (2019) 275–290, <https://doi.org/10.1016/j.biori.2019.09.001>.
- [28] W. Qian, W. Haiqing, C. Jin, K. Yan, Spherical V-Fe-MCM-48: the synthesis, characterization and hydrothermal stability, *Mater* 8 (2015) 1752–1765, <https://doi.org/10.3390/ma8041752>.
- [29] D. Tian, Y. Chen, X. Lu, Y. Ling, B. Lin, Facile Preparation of mesoporous MCM-48 containing silver nanoparticles with fly ash as raw materials for CO catalytic oxidation, *Micromachines* 12 (2021) 841, <https://doi.org/10.3390/mi12070841>.
- [30] K.S.W. Sing, D.H. Everett, R.A.W. Haul, L. Moscou, R.A. Pierotti, J. Rouquerol, T. Siemieniowska, Reporting physisorption data for gas/solid systems with special reference to the determination of surface area and porosity, *Pure Appl. Chem.* 57 (1985) 603–619, <https://doi.org/10.1351/pac198557040603>.
- [31] I.A. Lemus, Y.V. Gómez, L.Á. Contreras, Platinum nanoparticles synthesis supported in mesoporous silica and its effect in MCM-41 lattice, *Int. J. Electrochem. Sci.* 6 (2011) 4176–4187, <http://www.electrochemsci.org/papers/vol6/6094176.pdf>.
- [32] G. Mistura, A. Pozzato, G. Greci, L. Bruschi, M. Tormen, Continuous adsorption in highly ordered porous matrices made by nanolithography, *Nat. Commun.* 4 (2013) 2966, <https://doi.org/10.1038/ncomms3966>.
- [33] L. Qi, X. Tang, Z. Wang, X. Peng, Pore characterization of different types of coal from coal and gas outburst disaster sites using low temperature nitrogen adsorption approach, *Int. J. Min. Sci. Technol.* 27 (2017) 371–377, <https://doi.org/10.1016/j.ijmst.2017.01.005>.
- [34] F.J. Sotomayor, K.A. Cychosz, M. Thommes, Characterization of micro/mesoporous materials by physisorption: concepts and case studies, *Acc. Mater. Surf. Res.* 3 (2018) 34–50, [https://www.hyomen.org/en/wp-content/uploads/papers/vol3\\_no2/sotomayor/sotomayor\\_40.pdf](https://www.hyomen.org/en/wp-content/uploads/papers/vol3_no2/sotomayor/sotomayor_40.pdf).
- [35] H. Suo, H. Duan, C. Chen, J.C. Buffet, D. O'Hare, Bifunctional acid–base mesoporous silica@aqueous miscible organic-layered double hydroxides, *RSC Adv. Issue 7* (2019) 3749–3754, <https://doi.org/10.1039/C9RA00188C>.
- [36] P. Qin, Y. Yang, X. Zhang, J. Niu, H. Yang, S. Tian, J. Zhu, M. Lu, Highly efficient, rapid, and simultaneous removal of cationic dyes from aqueous solution using monodispersed mesoporous silica nanoparticles as the adsorbent, *Nanomaterials* 8 (2017) 4, <https://doi.org/10.3390/nano8010004>.
- [37] Q. Qin, J. Ma, K. Liu, Adsorption of nitrobenzene from aqueous solution by MCM-41, *J. Colloid Interface Sci.* 315 (2007) 80–86, <https://doi.org/10.1016/j.jcis.2007.06.060>.
- [38] J. Febrianto, A.N. Kosasih, J. Sunarso, Y.H. Ju, N. Indraswati, S. Ismadji, Equilibrium and kinetic studies in adsorption of heavy metals using biosorbent: a summary of recent studies, *J. Hazard Mater.* 162 (2009) 616–645, <https://doi.org/10.1016/j.jhazmat.2008.06.042>.
- [39] A.M.D. Jesus, L.P.C. Romão, B.R. Araújo, A.S. Costa, J.J. Marques, Use of humin as an alternative material for adsorption/desorption of reactive dyes, *Desalination* 274 (2011) 13–21, <https://doi.org/10.1016/j.desal.2011.01.063>.
- [40] T.S. Khayyun, A.H. Mseer, Comparison of the experimental results with the Langmuir and Freundlich models for copper removal on limestone adsorbent, *Appl. Water Sci.* 9 (2019) 170, <https://doi.org/10.1007/s13201-019-1061-2>.
- [41] L.C. Juang, C.C. Wang, C.K. Lee, Adsorption of basic dyes onto MCM-41, *Chemosphere* 64 (2006) 1920–1928, <https://doi.org/10.1016/j.chemosphere.2006.01.024>.
- [42] S. Wang, H. Li, L. Xu, Application of zeolite MCM-22 for basic dye removal from wastewater, *J. Colloid Interface Sci.* 295 (2006) 71–78, <https://doi.org/10.1016/j.jcis.2005.08.006>.
- [43] P. Baroni, R.S. Veira, E. Meneghetti, M.G.C. da Silva, M.M. Beppu, Evaluation of batch adsorption of chromium ions on natural and crosslinked chitosan membranes, *J. Hazard Mater.* 152 (2008) 1155–1163, <https://doi.org/10.1016/j.jhazmat.2007.07.099>.
- [44] A.S. Özcan, A. Özcan, Adsorption of acid dyes from aqueous solutions onto acid-activated bentonite, *J. Colloid Interface Sci.* 276 (2004) 39–46, <https://doi.org/10.1016/j.jcis.2004.03.043>.
- [45] A. Torabinejad, N. Nasirizadeh, M.E. Yazdandshenas, H.A. Tayebi, Synthesis of conductive polymer-coated mesoporous MCM-41 for textile dye removal from aqueous media, *J. Nanostructure Chem.* 7 (2017) 217–229, <https://doi.org/10.1007/s40097-017-0232-7>.
- [46] A.Q. Selim, E.A. Mohamed, M. Mobarak, A.M. Zayed, M.K. Seliem, S. Komarneni, Cr(VI) uptake by a composite of processed diatomite with MCM-41: isotherm, kinetic and thermodynamic studies, *Microporous Mesoporous Mater.* 260 (2018) 84–92, <https://doi.org/10.1016/j.micromeso.2017.10.041>.
- [47] G. Blanchard, M. Maunay, G. Martin, Removal of heavy metals from waters by means of natural zeolites, *Water Res.* 18 (1984) 1501–1507, [https://doi.org/10.1016/0043-1354\(84\)90124-6](https://doi.org/10.1016/0043-1354(84)90124-6).
- [48] J. Zhang, Z. Shen, W. Shan, Z. Mei, W. Wang, Adsorption behavior of phosphate on lanthanum(III)-coordinated diamino- functionalized 3D hybrid mesoporous silicates material, *J. Hazard Mater.* 186 (2011) 76–83, <https://doi.org/10.1016/j.jhazmat.2010.10.076>.
- [49] S.O. Akpotu, B. Moodley, MCM-48 encapsulated with reduced graphene oxide/graphene oxide and as-synthesised MCM-48 application in remediation of pharmaceuticals from aqueous system, *J. Mol. Liq.* 261 (2018) 540–549, <https://doi.org/10.1016/j.molliq.2018.04.046>.